Equilibrium and Kinetics Analysis of Carbon Dioxide Capture using Immobilized Amine on a Mesoporous Silica

Esmail R. Monazam
National Energy Technology Laboratory, REM Engineering Services, PLLC, Morgantown, WV 26505

Lawrence J. Shadle and David C. Miller
National Energy Technology Laboratory, U. S. Dept. of Energy, Morgantown, WV 26507

Henry W. Pennline, Daniel J. Fauth, James S. Hoffman, and McMahan L. Gray
National Energy Technology Laboratory, U. S. Dept. of Energy, Pittsburgh, PA 15236

DOI 10.1002/aic.13870
Published online July 23, 2012 in Wiley Online Library (wileyonlinelibrary.com).

Thermogravimetric analysis is used to study the adsorption kinetics, equilibrium, and thermodynamics of CO_2 on immobilized polyethylenimine sorbent impregnated on a mesoporous silica over the range of 300–390 K and 5–100% CO_2 concentration. Adsorption isotherm models were fitted to the experimental data indicating that a change in adsorption mechanism occurred near 70°C. Below this temperature, the adsorption data followed the heterogeneous isotherms, while data taken at higher-temperatures followed isotherms for homogeneous surfaces. Heat of sorption was estimated to be 130 kJ/mole for the low-temperature regime, but this decreased to 48 kJ/mole above 70°C. The rate of CO_2 fractional uptake decreased as temperature increased. A phenomenological kinetic model was derived from the Weibull distribution function using a nucleation growth theory to describe the two-step process. The kinetic model was used to predict the uptake at different operating conditions and resulted in good agreement with experimental data. Published 2012 American Institute of Chemical Engineers *AIChE J,* 59: 923–935, 2013
Keywords: adsorption/gas, reaction kinetics, green engineering, environmental, engineering, nucleation

Introduction

Coal-fired power plants produce and release carbon dioxide (CO_2) to the atmosphere, a major greenhouse gas contributing to global climate change. Given the growing global energy demand with fossil fuels as primary sources of energy, substantial measures are necessary to stabilize atmospheric CO_2. One method to achieve CO_2 mitigation, and still use fossil fuel, is to capture and store CO_2 from flue gas after combustion.[1] Currently, CO_2 separation can be performed by several approaches including absorption into liquid solvents, permeation through membranes, adsorption onto solids, and chemical conversion.[2] Researchers at the Department of Energy's National Energy Technology Laboratory have developed a high adsorption capacity sorbent by immobilizing amine functional group(s), such as those found in polyethylenimine (PEI). PEI can contain a mixture of primary, secondary, and/or tertiary amines and in dry conditions, the main reaction between amine and CO_2 is the formation of carbamate

$$\begin{aligned} 2RNH_2 + CO_2 &\leftrightarrow RNH_3^+ + RNHCOO^- \\ 2R_2NH + CO_2 &\leftrightarrow R_2NH_2^+ + R_2NCOO^- \\ R_3N + CO_2 + R'NH_2 &\leftrightarrow R_3NH^+ + R'NHCOO^- \end{aligned} \quad (1)$$

These are grafted on high surface area supports such as mesoporous silicas.[3] This high surface area support immobilizes a large number of active amine sites per gram of support. The nature of the amine functional groups determines the amount of CO_2 adsorbed and the energy required for regenerating the sorbent.

Solid sorbents, such as zeolites, aminated mesoporous silica, and activated carbons, have been extensively used for CO_2 capture from various sources.[4–8] However, very few kinetic and equilibrium data are available for these promising sorbents.[9,10] In the solid–gas reaction, determination of the kinetic equation, rate controlling steps, and kinetic parameters provide valuable insight into the mechanism of the process. To optimize the design of an adsorption system removing CO_2 from flue gases, it is also important to establish the most appropriate expression for the equilibrium data. A relationship describing equilibrium data, using either a theoretical or an empirical equation, is essential to interpret and predict the extent of adsorption. Thus, the objective of this article is to determine the kinetics, equilibrium, and thermodynamic parameters of the CO_2 removal by an immobilized amine on high surface area mesoporous silica material.

Experiment

Materials

Methanol (reagent grade) and PEI (MW_N 423) used in the preparation of the immobilized sorbents were purchased from Sigma-Aldrich Chemical and used without purification.

Correspondence concerning this article should be addressed to L. J. Shadle at lshadl@netl.doe.gov.

Table 1. Physical Properties of Substrates[11]

Substrate	Chemical Backbone	Surface Area (m^2/g)	Pore Volume (ml/g)	Particle Size (μm)
Macronet	Polystyrene	1000	1.0	1130–300
CARiACT	Silicon dioxide	300	1.3	75–150
Diaion	Polymethyl-methacrylate	470	1.2	200–400

The silica substrate selected in this investigation was CARiACT®G10 from Fuji Silysia Chemical. The physical properties of this substrate are summarized in Table 1 along with a polystyrene support, polymethy-methacrylate as used in the past studies.[11] In this study, the CARiACT substrate was selected based on suitability of the particle size for a fluidized bed reactor configuration. This material has a mean size of 80 μm.

Preparation

The amines were dissolved in methanol and combined with the silica beads at a 0.67 amine/2.0 methanol/1.0 bead weight ratio. This bead slurry was then placed in a rotary evaporator, and the methanol was removed, resulting in the physical adsorption (immobilization) of the amine into these beads. Details of this method are given in the patent by Birbara et al.,[11] which describes impregnating amines on high surface area substrates similar to those shown in Table 1. A nominal total of 40% PEI by weight was immobilized onto the substrate, and then the CO_2 capture sorbent was tested using thermogravimetric method. The impregnation procedure produces a well-distributed layer of PEI on mesoporous silica substrates.[12] Xu et al.[12] describe a synergistic influence of the PEI with the mesoporous substrate such that the adsorption capacity in the "molecular basket" increases over that observed for either individually when PEI loadings exceed 20% by weight. The synergistic effect maximizes at 50% PEI loading and this is described as the optimal distribution of PEI on the mesoporous surface. PEI coats the external surface creating a layer exhibiting CO_2 diffusion resistance when PEI loadings exceed 75%.

Testing

A Thermo Cahn Thermomax 300 unit thermogravimetric analyzer (TGA) was used to examine the fundamental kinetics of CO_2 uptake information using immobilized PEI sorbent. This apparatus has a reaction chamber volume of less than 30 ml. For a typical test, a 30 mg of sample was placed in the microbalance quartz sample bowl. Drying under an inert flow of nitrogen preceded the adsorption step. The adsorption was conducted within the temperature range of 40–100°C and five CO_2 concentrations: 5, 10, 20, 50, and 100% with the balance nitrogen. The weight of the sorbent sample and the reaction temperature were recorded continuously. In all experiments, the flow rate of reactant gas (CO_2) and inert gas (N_2) were set at 100 ml/min (at standard rate) supplied by Butler Gas Supply of Pittsburgh, Pa with stock gas grade 99.99% purity. The sample size, gas flow rate, and particle size were optimized to minimize measurement artifacts due to dispersion and mass transfer of CO_2 to the sorbent particles. At the end of adsorption step, the sorbent was again exposed to a flow of nitrogen at 105°C to regenerate the sample. A further ramp in temperature to 600°C under inert was conducted to drive off all organic material from the silica substrate and, thus, determine the loading of the

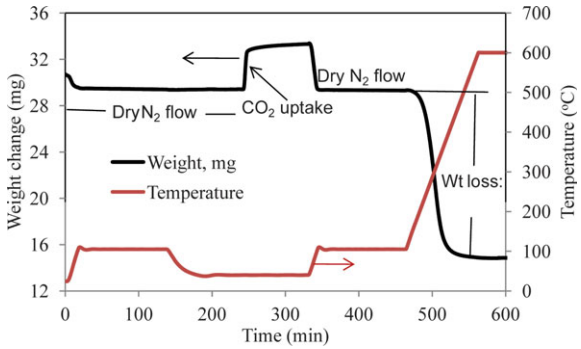

Figure 1. Typical temperature and mass measurements during TGA experiment (10% CO_2, 40°C).

[Color figure can be viewed in the online issue, which is available at wileyonlinelibrary.com.]

PEI on the sorbent. A typical experimental observation for temperature and changes in weight during TGA experiments is illustrated by Figure 1 (10% CO_2, 40°C).

The required data acquisition rate was determined by varying the sampling rate. The data acquisition rate was varied from 5 to 2 s per sample to evaluate the influence of time resolution. The sampling rate tests were conducted at 40°C, 100% CO_2 flowing at 100 sccm over nominally 15 mg sample of sorbent. Under these conditions, 80% of the CO_2 uptake occurred within 30 s of gas switching, therefore, the slower sampling rate produced only 6 data points. The higher sampling rate produced 15 data points over the same period, 2 and $^1/_2$ times the resolution. It was decided that the higher sampling rate was a significant improvement and so it was applied for all subsequent tests. In all other respects, these data sets represented replicates. The repeatability was determined by adjusting the fixed error on the uptake normalized to a maximum of unity (X) until the measured sorption $\pm$ error overlapped both repeats over the entire test duration. The uncertainty was found to be $\pm$0.02 or a fixed value of 2% of the eventual asymptotic uptake level. This error is depicted on Figure 2 as error bars on the high and low gas flow tests.

To define the test conditions in which heat and mass transfer through the packed bed of samples were not controlling

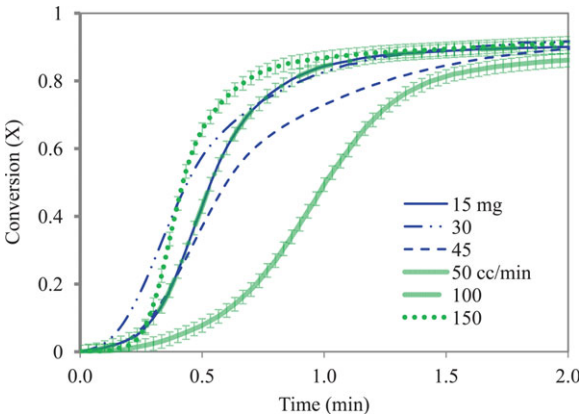

Figure 2. The effect of sample size and gas flow rate on the normalized CO_2 uptake at 100% CO_2 and 60°C.

[Color figure can be viewed in the online issue, which is available at wileyonlinelibrary.com.]

Table 2. Gas Flow and Sample Size Effects on Conversion Rate Related Parameters

Trial No.	Sample Wt (mg)	Gas Flow (sccm)	$dX/dt\|_{max}$ (min^{-1})	$t_{dXdt\|max}$ (min)	t_{50} (min)
1	49.0450	100	**1.40**	0.467	**0.642**
2	33.6436	100	1.75	0.333	**0.622**
3	16.1874	100	1.95	0.500	0.505
Std Error=			*0.16*	*0.051*	*0.043*
4	17.2144	150	3.08	0.400	0.333
3	16.1874	100	1.95	0.500	0.505
5	16.1478	50	1.17	**0.967**	0.626
Std Error=			*0.55*	*0.175*	*0.085*

the uptake of CO_2, several experiments were conducted on gas flow rates and sample size. The gas flow was varied from 50, 100, to 150 sccm at 15 mg sample size. The sample size was varied from 15 up to 45 mg while holding the gas flow rate at 100 sccm. For these tests, the temperature was constant at 60°C and 100% CO_2 concentration was used. It was found that the lower gas flow tended to slow the uptake of CO_2 (Figure 2). Using the same approach for quantifying significance as in the uptake repeatability tests, all of the changes in gas flow and sample size were significant based on the error associated with repeat tests available; however, the relative differences were sufficient to discern the impacts and determine optimal test conditions. For instance, there was only 13% fixed error required to overlap all of the 100 and 150 sccm test data, while uncertainty of 50% error was required to overlap the 50 and 100 sccm test results. A reasonable flow of 100 sccm was selected as the optimal compromise between excess gas flows and mass transfer effects.

The effect of sample size was not so distinct. The 45 mg uptake data was slower after the peak uptake, while the 15 mg uptake data was faster before the peak uptake. The sample size data required error of only 15% of the maximum uptake to overlap the entire uptake curve pairwise for each adjacent data set, 15 with 30 mg and 30 with 45 mg. Thus, the uncertainty in these experiments was characterized as ±15% of the maximum uptake.

The influences of gas flows and sample size on rates were also evaluated quantitatively using three dependent parameters taken directly from the derivative of the uptake curves with respect to time: (1) the maximum rate, $dX/dt|_{max}$, (2) the time corresponding to this maximum rate, $t_{dx/dt|max}$, and (3) the breadth of this rate curve as characterized by the width at half height, t_{50}. The data and analysis results are presented in Table 2. In general, the rates parameters indicated a faster uptake process with smaller sample and higher gas flow rates indicating that the tests were conducted over a range where heat or mass transfer to the particles influenced the rates. If there were strong transfer effects to the uptake process then a systematic trend would be expected in these rate parameters with changes in the independent variable. A systematic trend was found in all of these rate parameters for the gas flow tests, but this was not true for variations in the sample size. This indicated that the variations in sample size were less repeatable and the mass transfer effect was less significant than that produced from the variations in the gas flow. The standard error from the mean was used to test differences. The measured rate parameters were compared pairwise for adjacent test conditions. When these values for the dependent parameters were different by more than twice the standard error, then the values were considered significant. Unlike to the analysis of the time series data, none of the rate parameters estimated in Table 2 produced a significant difference between 100 and 150 sccm, while the $t_{dx/dt|max}$ was much greater than twice the standard error for the 50 as compared to the 100 sccm test. This confirmed the selection of 100 sccm for gas flows and indicates that mass and heat transfer to the particles did not significantly impact the rates.

When analyzing the effect of sample size on these rate parameters, the smallest sample size significantly reduced the spread in the uptake rate as measured by t_{50}. Since the smallest sample size reduced the amount of potential mass transfer effects, and smaller samples would not impact the accuracy of the weight loss measurements, it was decided to use 15 mg sample size for all subsequent testing. Thus, the analysis conducted on sample size and gas sweep rate did demonstrate the lack of heat mass transfer effects to the particles.

Theory

The equilibrium sorption isotherm is crucial for the design of sorption systems. Equilibrium sorption is usually described by an isotherm equation characterized by certain parameters whose values express the surface properties and affinity of the sorbent. The equilibrium relationships between sorbent and sorbate are described by sorption isotherms, the ratio between the amount adsorbed and that remaining in the reactant at a fixed temperature at equilibrium. In this study, for investigating the sorption isotherm, four commonly used adsorption models, namely Langmuir, Temkin, Freundlich, and Dubinin–Radushkevich (D–R) isotherms were applied to evaluate feasibility of adsorbate–adsorbent interaction (Table 3).

Langmuir isotherm

The Langmuir equation is probably the best known and most widely used adsorption isotherm.[13,14] The mathematical expressions for the Langmuir isotherm are given in Table 3. This isotherm was developed on the premise that adsorption sites are homogeneous in nature where the sorption of each sorbate molecule onto the surface has nearly equal sorption energy. The essential parameter in the Langmuir isotherms is a dimensionless constant, the separation factor or equilibrium parameter, R_L, which is defined as

Table 3. Lists of Adsorption Isotherms Models

Isotherm	Nonelinear Form	Linear Form	Plot	References
Langmuir	$q_e = \frac{q_m K_L C_{CO_2}}{1 + K_L C_{CO_2}}$	$\frac{C_{CO_2}}{q_e} = \frac{1}{q_m K_L} + \frac{C_{CO_2}}{q_m}$	C_{CO2}/q_e vs. C_{CO_2}	13 and 14
Temkin	$q_e = B \ln(K_T C_{CO_2})$	$q_e = B \ln(K_T) + B \ln(C_{CO_2})$	q_e vs. $\ln C_{CO_2}$	13 and 15
Freundlich	$q_e = K_F C_{CO_2}^{1/n}$	$\ln q_e = \ln K_F + \frac{1}{n} \ln C_{CO_2}$	$\ln q_e$ vs. $\ln C_{CO_2}$	13 and 15
Dubinin–Radushkevich	$q_e = q_m e^{-\lambda \omega^2}$	$\ln q_e = \ln q_m - \lambda \omega^2$	$\ln q_e$ vs. ω^2	16

$$R_L = \frac{1}{1 + K_L C_{CO_2,0}} \quad (2)$$

where $C_{CO_2,0}$ is the initial CO_2 concentration. The value of R_L indicates the shape of the isotherm[13] ($R_L > 1$ unfavorable; $R_L = 1$ linear; $R_L = 0$ irreversible; $0 < R_L < 1$ favorable).

Temkin isotherm

The Temkin isotherm describes the behavior of adsorption systems on heterogeneous surfaces, and assumes that (1) the heat of adsorption of all molecules in the layer would decrease linearly with coverage due to adsorbent–adsorbate interactions, and that (2) the adsorption is characterized by a uniform distribution of binding energies, up to some maximum binding energy.[17,18]

Freundlich isotherm

The Freundlich isotherm can be applied to non-ideal adsorption on heterogeneous surfaces as well as multilayer sorption.[13,15] The slope, $1/n$, of the linear expression in Table 3 ranges between 0 and 1 is a measure of adsorption intensity or surface heterogeneity. Values of $1/n = 0$ indicates that the partition between two phases does not depend on the concentration; $1/n < 1$ corresponds to a normal L-type Langmuir isotherm, while $1/n > 1$ indicates a cooperative sorption involving strong interactions between the molecules of adsorbate.[19]

Dubinin–Radushkevich isotherm

The Dubinin–Radushkevich (D–R) isotherm can be used to describe adsorption on both homogenous and heterogeneous surfaces.[16] The D–R equation is listed in Table 3 and the parameter ω is the Polanyi potential that is related to the equilibrium by

$$\omega = RT \ln\left(1 + \frac{1}{C_{CO_2}}\right) \quad (3)$$

where, R is the gas constant (8.314 J/mol K) and T is the absolute temperature. Meanwhile, the constant λ gives the mean free energy, E, of adsorption when it is transferred to the surface of the solid from infinity in the gas. The mean free energy adsorbed per molecule adsorbate can be computed using the relationship[20]

$$E = \frac{1}{\sqrt{2\lambda}} \quad (4)$$

The magnitude of E is useful for estimating the mechanism of the adsorption reaction. In the case of $E < 8$ kJ/mol, physical forces may affect the adsorption. If E is in the range of 8–16 kJ/mol, adsorption is governed by ion exchange mechanism, while for the values of $E > 16$ kJ/mol, adsorption may be dominated by particle diffusion.[21]

Adsorption kinetics

For the purpose of determining the rate equation, it was assumed that "X" is the fraction of sites which are occupied by adsorbed gas

$$X = \frac{q_t}{q_e} = \frac{\frac{(m(t)-m_0)}{m_0}}{\frac{(m_f-m_0)}{m_0}} = \frac{(m(t)-m_0)}{(m_f-m_0)} \quad (5)$$

where $m(t)$ is instantaneous weight of the solid during the exposure to CO_2. Parameters m_0 and m_f are initial and final weight of the sorbent, respectively.

The differential kinetic equation can be expressed as[22]

$$\frac{dX}{dt} = k(T) f(X) \quad (6)$$

where the rate constant $k(T)$ can be replaced with the Arrhenius equation, yielding

$$\frac{dX}{dt} = A \exp\left(\frac{E}{RT}\right) f(X) \quad (7)$$

The function $f(X)$ is an analytical expression describing the kinetic model. In isothermal experiments, the Arrhenius equation is constant and the reaction rate, dX/dt, is proportional to the $f(X)$ function. Therefore, when the reaction rate is plotted as a function of X, its shape corresponds to the $f(X)$ function.[23] The shape of this plot is characteristic for each kinetic model and it can be used as a diagnostic tool for the kinetic model determination. For isothermal data, an appropriate kinetic model can be determined by evaluating the nature of uptake rate data. One of the following plots must be generated: plot either dX/dt vs. X, or plot $\ln(X)$ or $\ln(dX/dt)$ vs. time.[24] The resulting curve can have one of the following two features:

Case 1. *If the reaction rate curve has a maximum at $X = 0$ or $t = 0$, then the order of the reaction can be evaluated from the shape of the curve (i.e., linear, concave, or convex). A linear relationship is indicative of a first-order reaction process. Concave and convex shape curve requires a more complicated model. If the plot is concave upward, the reaction model could be either nth-order reaction with $n > 1$ or a multiexponential decay having anywhere from two to a continuous distribution of rate constants. If the plot is concave downward, either an nth-order model with $n < 1$, a serial model, or a nucleation model is applicable.*

Case 2. *The second case is when the reaction rate does not achieve the maximum at $X = 0$ or $t = 0$, and the rate rises due to the intrinsic chemical kinetics or to measurement artifacts. An intrinsic chemical kinetic model should be used to describe the peaked shape rate curve. When the initial reaction rate is zero at $t = 0$, a sigmoidal or autocatalytic model such as a nucleation reaction model can be used to characterize the rate curve.*[25] *On the other hand, the initial rise could be due to transport through a porous material from either heat transfer or mass transfer through the particle. Transfer of heat to sorbent and mixing of the sorbate must be eliminated as causes for this behavior. Finely sized sorbent particles are used to minimize the possible effect of the measurement artifact.*[26]

Therefore, the shape of dX/dt functions can be used conveniently for the determination of the most probable kinetics model.[27]

Results and Discussion

CO_2 capture capacity

The CO_2 concentration plays an important role in the whole adsorption process and particularly on the adsorption capacity. Figure 3 shows the adsorption capacity, q_e, of immobilized PEI/silica sorbent with increasing CO_2 mole fraction. The experimental CO_2 loading was determined for five CO_2 concentrations and five temperatures (Figure 3). The 50°C data were in between 40 and 60°C data and so is not reproduced on Figure 3. The relative weight gain in the

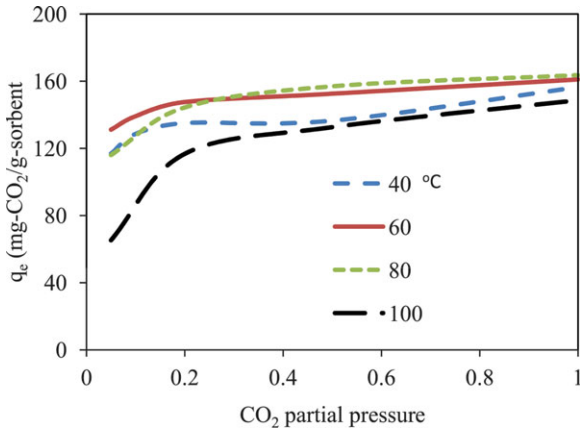

Figure 3. Experimental variation of maximum CO_2 loading with temperature and CO_2 partial pressure.

[Color figure can be viewed in the online issue, which is available at wileyonlinelibrary.com.]

thermogravimetric tests after the 90 min holding period was taken as pseudo-equilibrium loading (mg CO_2/g sorbent). The weight change in the last 5 min was invariably found to be less than 1% of the overall weight change. The values of the pseudo-equilibrium loading, q_e, increased with increasing CO_2 concentration for each reaction temperature. The CO_2 concentration provides the necessary driving force to overcome the resistances to the mass transfer of CO_2 between the CO_2 and solid phases. The increase in CO_2 concentration also improves the ability for CO_2 to interact with the solid supported amine. It was observed that an increase in concentration of CO_2 enhanced the adsorption uptake of CO_2. On the other hand, the adsorbed CO_2 was not released in significant quantities, that is, the sorbent regenerated, until the concentration of CO_2 dropped below 20%. A more rapid loss in sorbent capacity was only observed at the highest temperature, 100°C. The lower-temperatures maintained a rather shallow drop in capacity even for low CO_2 concentrations (5% vol).

In general, the sorbent capacity was a maximum between 60 and 80°C and was lower than that for 40 and 100°C. Ma et al.[28]explain that the lower capacity at 40°C is due to a higher kinetic barrier for diffusion into the deeper multilayers of PEI when loaded on mesoporous silica. They conclude that diffusion of the CO_2 adsorbed from the surface into the bulk of PEI reduces the total number of the accessible sorption sites for CO_2 at 40°C, even though low-temperature thermodynamically favors the adsorption of CO_2 on the surface of PEI. This may be due to the increased ordering, perhaps crosslinking, of the polyamine with the adsorbed CO_2. It is reported that viscosity of ionic amine liquids increase in viscosity as they adsorb CO_2 as a result of the CO_2 forming a strong pervasive hydrogen bonded network limiting translational and rotational dynamics.[29] Such networks were reported to generate gel-like and glassy products which can be thought to contribute to mass transfer barriers. Ma et al.[28] reported this reduction in sorbent capacity as significant for mesoporous sorbent loaded with 50% PEI. The sorbent used in this study was only loaded with 40% PEI, and the reduction in capacity at 40°C compared to 60 or 80°C was apparent, though not significantly so (Figure 3). This is consistent with observation by Xu et al.[12] for 40% PEI loaded adsorbent. The lower PEI loading onto the mesoporous substrate likely reduced, but did not eliminate, the mass transfer restrictions to the deeper layers of PEI at low-temperatures.

At temperatures above 70°C, the CO_2 sorption capacity dropped (Figure 3), as the control of the sorption shifts from the diffusion kinetic regime to the thermodynamic regime. According to Ma et al.,[28] the increase in temperature facilitates the mass transfer of the adsorbed CO_2 molecules from the surface into the bulk of PEI by overcoming a diffusion kinetic barrier. This leads to the observed enhancement of the total number of the accessible sorption sites at 80°C. Ma et al.[28] report quantum calculations that indicate the high heat of sorption for CO_2 creates a sufficient deep potential well at 80°C to maintain an affinity for CO_2 and capture it. The immobilized PEI sorbent exhibited a higher sorption capacity for CO_2 at 80°C than at 40°C.

Adsorption isotherms

To optimize the design of CO_2 adsorption system it is important to establish the appropriate mechanisms and quantitatively describe the thermodynamic equilibrium. Hence, understanding the equilibrium data is essential to predict the adsorption behavior. Therefore, the equilibrium experimental data for adsorbed CO_2 on immobilized PEI/silica sorbent were analyzed using the Langmuir, Temkin, Freundlich, and Dubinin–Radushkevich (D–R) isotherms in this study.

The adsorption data were analyzed according to the linear forms of the Langmuir, Temkin, Freundlich, and D–R isotherms (Table 3). The values of the Langmuir constants K_L and q_m, Temkin constants K_T and B, Freundlich constants K_F and n, and D–R constants λ and ω with correlation coefficients for different temperatures are listed in Table 4. Figure 4 display a comparison of the experimental data (q_e vs. CO_2 mole fraction) with the Langmuir, Temkin, Freundlich, and D–R at 40 and 100°C. At lower-temperature, the Langmuir and D–R model did not fit the observed increase in pseudo-equilibrium capacity with increased CO_2 concentration (Figure 4A). At higher-temperature, the Langmuir and D–R model fit the best compared to Temkin and Freundlich model (Figure 4B).

For Langmuir-type adsorption process, the isotherm shape can be classified by a dimensionless constant separation factor, R_L, (Eq. 2). The calculated R_L values for different CO_2 concentration at given temperatures are displayed in Figure 5. The values of R_L in the range of 0–1 confirmed that CO_2 uptake was favorable using immobilized PEI/silica sorbent. Also, lower R_L values at higher CO_2 concentrations showed that adsorption was less reversible at higher CO_2 concentration. The degree of favorability tended toward zero (the completely ideal irreversible case) rather than unity (which represents a completely reversible case).

Overall, the CO_2 adsorption was best described by the Temkin and Freundlich isotherms. The constant b_T in the Temkin isotherm reflects bonding energy which in turn dictates the type of interaction. The low values obtained (0.1–0.25 kJ/mol) indicate that interactions between the sorbate and sorbent are neither purely ion exchange nor purely physisorption.[30] Higher values are indicative of ion exchange while lower values are indicative of physisorption processes. Typical bonding energy range for ion-exchange mechanism is reported to be 8–16 kJ/mol.[31] It is observed that up to −20 kJ/mol is surface indicative of physisorption process

Table 4. Langmuir, Temkin, Freundlich, and Dubinin–Radushkevich Isotherm Constants

Langmuir				Temkin			
T (K)	K_L (CC/mg)	q_m (mg/g)	R^2	B	K_T (CC/mg)	b_T (kJ/mole)	R^2
313	18.76	170.13	0.871	13.95	83047	0.186	0.999
323	25.68	172.32	0.915	12.45	481850	0.215	0.991
333	28.18	172.83	0.965	11.39	1797670	0.243	0.987
353	22.75	169.18	0.985	16.48	17746	0.178	0.98
373	9.69	159.85	0.999	27.56	193	0.112	0.965
Freundlich				Dubinin–Radushkevich			
T (K)	$1/n$ (CC/mg)	K_F (mg/g)	R^2	b	q_m (mg/g)	E (kJ/mole)	R^2
313	0.0965	157.76	0.999	6.36E−09	160.26	12.54	0.903
323	0.083	161.85	0.992	5.15E−09	164.33	13.93	0.924
333	0.0747	164.70	0.989	4.26E−09	166.40	15.32	0.94
353	0.1174	161.50	0.98	5.97E−09	164.25	12.94	0.988
373	0.2634	147.42	0.968	1.19E−08	153.07	9.15	0.996

due to electrostatic interaction between charged molecules whereas more negative than −40 kJ/mol involves chemisorption.[32]

The Freundlich isotherm also fit the experimental data quite well. The linear Freundlich isotherm constants K_F and $1/n$ are presented in Table 4. The Freundlich isotherm parameter $1/n$ measures the adsorption intensity of CO_2 on the PEI/silica sorbent. The values of $1/n$ were found to be less than unity (0.07–0.26) indicating that the isotherms can be characterized as a favorable isotherm.[13,14]

The D–R constants are calculated and given in Table 4 and the theoretical D–R isotherm is plotted in Figure 4 together with the experimental data points. The correlation coefficients were determined for each isotherm and given along with the R^2 values. Overall, the values for R^2 were higher than that for the Freundlich but lower than both Langmuir and Temkin isotherms. However, the D–R equation generally represented a better fit of experimental data over the entire temperature range. Still, the D–R isotherm did not fit the data at low-temperature as well as either the Freundlich and Temkin isotherms and did not fit the high-temperature data quite as well as the Langmuir isotherm (Figure 3). The adsorption energy, E, determined from the D–R isotherm was found to be 9–15 kJ/mol. This value is within the range of those typical of an ion exchange process.

The sorption mechanism of CO_2 on PEI silica was found to vary as a function of temperature. At low-temperature (between 40 and 60°C), the isotherm models for heterogeneous adsorption sites, Temkin and Freundlich, were best suited to capture the variability in the experimental data. The Temkin isotherm indicated that the process was not

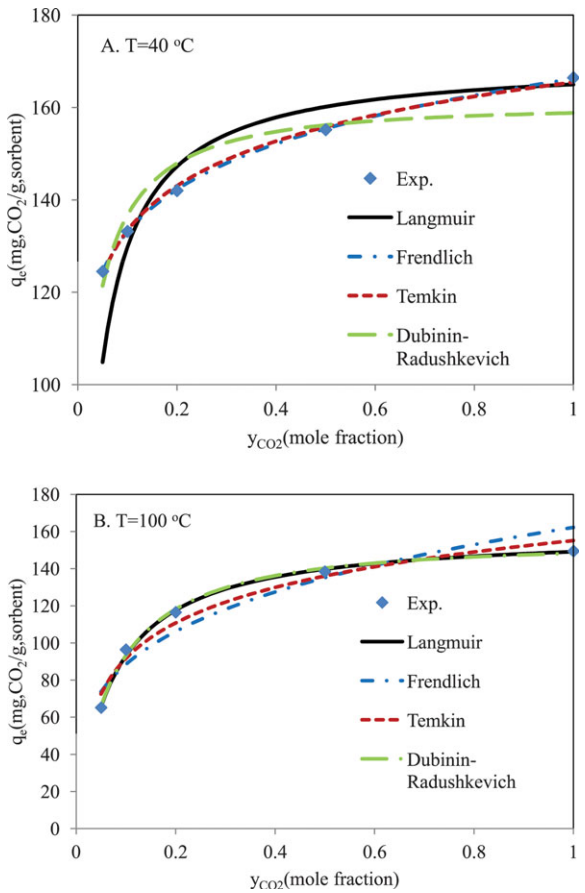

Figure 4. Sorption isotherms from TGA experiment over different CO_2 concentrations.

A) 40°C and B) 100°C. [Color figure can be viewed in the online issue, which is available at wileyonlinelibrary.com.]

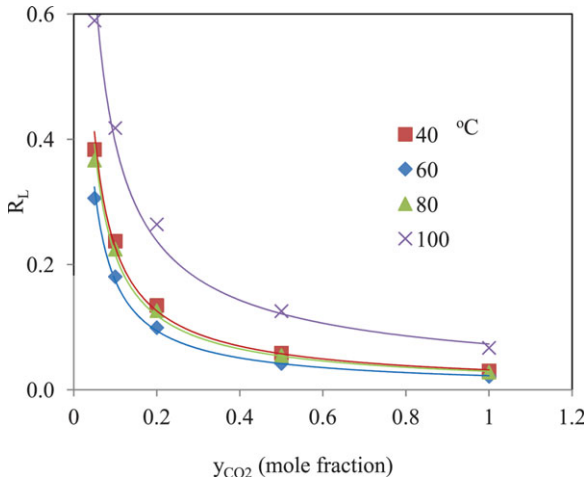

Figure 5. Langmuir's separation factor as a function of CO_2 concentrations for given temperatures.

[Color figure can be viewed in the online issue, which is available at wileyonlinelibrary.com.]

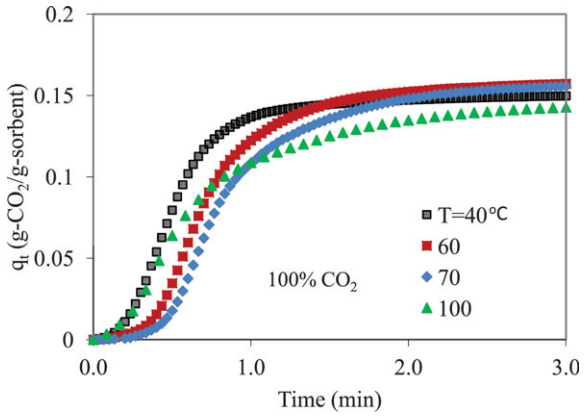

Figure 6. Effect of reaction temperature on CO_2 uptake for immobilized PEI sorbent particle and CO_2 reaction using 100% CO_2.

[Color figure can be viewed in the online issue, which is available at wileyonlinelibrary.com.]

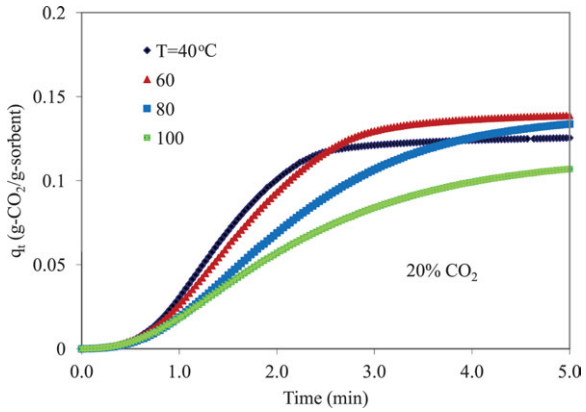

Figure 7. Effect of reaction temperature on CO_2 uptake for immobilized PEI sorbent particle and CO_2 reaction using 20% CO_2.

[Color figure can be viewed in the online issue, which is available at wileyonlinelibrary.com.]

fully physisorption or ion exchange with a bonding energy between 0.1 and 0.25 kJ/mol, while the Freundlich isotherm indicated that the sorption process was favorable. The Freundlich isotherm was used to estimate the theoretical maximum uptake to be from 157 to 165 mg CO_2/g sorbent. The heat of reaction was estimated to be 133 kJ/mole of CO_2 adsorbed over this lower-temperature range by plotting ln K_F from the Temkin isotherm against $1/T$.

At temperatures above 70°C, the Langmuir and D–R isotherms best explained the variability in the data indicating a more homogeneous active surface. At these temperatures, the heat of sorption was found to be 48 kJ/mol based upon the Langmuir isotherm. The D–R isotherm produced an adsorption energy of 9–13 kJ/mol leading to the conclusion that the adsorption mechanism of PEI on silica was an ion exchange process. The theoretical capacity for these higher-temperatures was similar to that at lower-temperatures estimated to be between 153 and 169 mg CO_2/g sorbent. In summary, analysis of the adsorption isotherms indicated that the adsorption process changes between 60 and 80°C.

Kinetic analysis

The TGA data on CO_2 sorption on immobilized PEI/silica sorbent are illustrated by Figure 6 at different reaction temperatures in 100% CO_2. The CO_2 adsorption capacity and uptake in g-CO_2/g-adsorbent (q) were calculated from the weight gain during adsorption of the sample per initial weight of adsorbent. It can be seen that CO_2 uptake increased monotonically with CO_2 exposure time and the sorbent reached saturation levels in about 2 min. The rapid uptake of CO_2 was preceded by an induction period that resulted in a sigmoidal shaped uptake curve with time typical of Case 2 kinetics. The extent of the induction period depended on the CO_2 concentration and sorption temperature. In an atmosphere with 100% CO_2, this induction time increased as temperature increased initially up to 70°C and then decreased again. The time required for the sorbent to reach saturation was longer at the higher-temperatures. Up to the maximum uptake at 70°C, the longer time to reach saturation was due to longer induction times; however, at 100°C, the longer uptake time was a result of slower approach to equilibrium after the initial rapid rise. The induction period was independent of temperature at lower CO_2 concentrations (Figure 7). The induction period was found to be approximately constant for CO_2 concentrations below 100%; however, the time required to reach saturation capacity was similar for all concentrations of CO_2 and the rate decreased with increasing temperature (Figures 8 and 9).

It is important to emphasize that the rate of CO_2 uptake decreased with increasing temperature. This can be better demonstrated by looking at the uptake rate as a function of time and temperature (Figures 8 and 9). The rates were derived by differentiating the data in Figures 6 and 7 for 100% and 20% CO_2 concentration. The rate-time curves for all the temperatures show that unlike simple first-order reactions, the maximum rate of process was obtained at $t > 0$. In general, the CO_2 uptake rate increased to a maximum and then decreased as the sorbent approached its saturation or pseudo-equilibrium levels. Prior to the peak, the rate of CO_2 uptake decreased with increasing temperature. After the peak, the temperature dependence was reversed at any point in time; the uptake rate increased with temperature.

Wang et al.[33] also reported similar observations for PEI(50)/SBA-15 sorbent. They indicated that there could be different rate-determining factors controlling CO_2 sorption over the sorbent at different sorption times. They indicate a

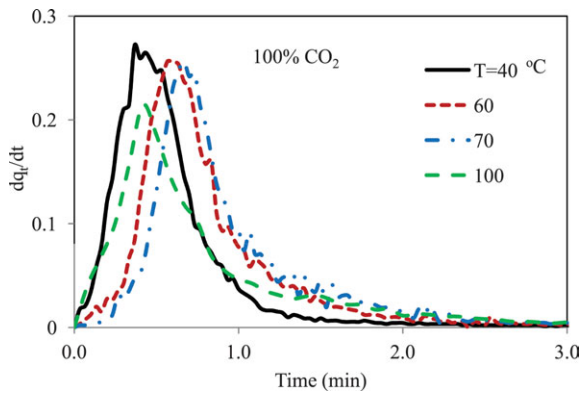

Figure 8. The differentiated CO_2 uptake for immobilized PEI sorbent particle and CO_2 reaction for different temperature using 100% CO_2.

[Color figure can be viewed in the online issue, which is available at wileyonlinelibrary.com.]

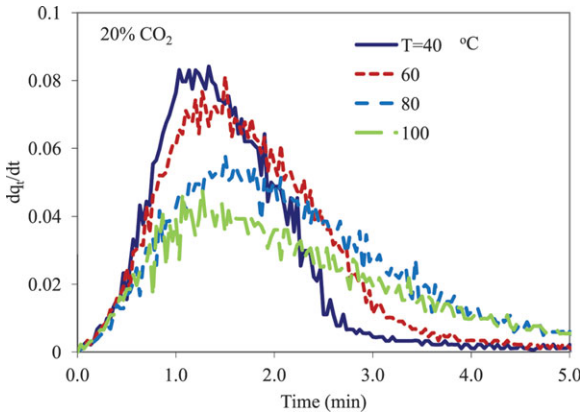

Figure 9. The differentiated CO_2 uptake for immobilized PEI sorbent particle and CO_2 reaction for different temperature using 20% CO_2.

[Color figure can be viewed in the online issue, which is available at wileyonlinelibrary.com.]

two-step process for CO_2 uptake into PEI in mesoporous sorbent. The first is the surface adsorption of CO_2, which is thermodynamically favored at lower-temperatures. The second step was reported to involve diffusion of CO_2 into the lower PEI multilayers. According to Wang et al., the first step dominates the rate prior to the peak while the second step dominates the rate following the peak.

In this study, the plots of CO_2 uptake rates (Figures 8 and 9) displayed characteristics of Case 2 kinetics. Initial attempts to fit the uptake data to single first-order and second-order reaction models displayed significant lack of fit. Transport processes between apparatus and the sorbent were not the cause of the sigmoidal shaped uptake curves. A similar study using comparable TGA equipment and procedures using clays impregnated with amines did not produce sigmoidal shaped uptake curves, but instead displayed Case 1 behavior (peak rate at time = 0).[9] The sigmoidal shape was not a result of heat transfer to the surface or mass transfer due to gas mixing on transitioning from inert to sorbate gas. Nevertheless, in this study, the fine sorbent particles, small sample size, and high gas flow rates were used to minimize the possible effect of these measurement artifacts as recommended.[26]

Development of Kinetic Expression. A Johnson–Mehl–Avrami (JMA) model is used extensively in the field of nucleation and growth.[34] The JMA model and the Weibull cumulative distribution function (CDF) displayed many of the necessary characteristics to explain the experimental observations for this type of sorbent. The Weibull function describes the decay rate of a lifetime process. It has the feature that has a memory in that the progress depends on the prior state. In the Weibull CDF,[35] the reaction times are randomly distributed and the reaction curve exhibits a sigmoidal shape. An equation similar to the Weibull distribution function was developed for the reaction time (t) proportional to the fractional uptake (X) according to

$$X(t) = 1 - e^{(-at^b)} \tag{8}$$

In the Weibull CDF, a is referred to as the scale parameter and b is the shape parameter. There is one notable difference between this and the Weibull functional form which includes exponential effect on the scale parameter, such that $X(t)$ is related to $(-at)^b$. In nucleation and crystallization kinetic analyses, a is described as a cluster of numerical and growth constants which are different in each reaction and b is considered the kinetic exponent. As a decreases, the slope of the curve increases and take a longer time to reach steady-state. In this study, the value of a was better fitted without the exponential dependence on the kinetic exponent, b. This may be due to the nature of the growth constants for this specific reaction. Similar findings are reported for crystallization kinetics.[36] As b increases, the uptake curve becomes steeper. According to diffusion controlled nucleation and growth theory, the magnitude of the shape factor reflects how the nucleation rate changes under isothermal conditions: 1.5 is a zero nucleation rate, 1.5 to 2.5 is a decreasing nucleation rate, 2.5 is a constant nucleation rate, and b values are greater than 2.5 for increasing nucleation rates.[34] This expression also is well suited to capture the observed temperature dependence with the induction period as described below.

The nucleation and growth mechanism offers some additional insight into this process. According to the nucleation and nuclei growth model,[34] the gas–solid reactions proceed by nucleation (nuclei formation) and subsequent growth of the nuclei. Before nucleation, there is a delay or induction period for the activation of the solid phase to form nuclei. The length of the induction period primarily depends on the gas–solid system and reaction temperature. Nucleation is a dynamic process, which occurs in a manner analogous to droplet formation from a supersaturated vapor mixture. In this case, it will be shown that CO_2 diffused uniformly throughout the particle until it had the opportunity to interact with and occupy an active amine site. A product nuclei or "droplet" is formed once a sufficient local concentration of occupied sites exceeds that necessary to produce stable product species such as carbamate. These product nuclei may be thought to form at the mouth of the cylindrical mesopores. The progress of the reaction continues with additional nucleation and growth of the already formed nuclei. The reaction of CO_2 at available active sites proceeds down the length of the mesopores and accounts for continued growth and CO_2 uptake. The overall rate of the adsorption is determined by the relative rate of nucleation, nuclei growth, and the concentration of the potential nucleus-forming sites known as germ nuclei. Either nucleation, nuclei growth, or their combination can be the rate-determining step of the overall reaction, and the energetics of the reaction process is primarily dependent on the rate-determining step.

Figure 10 compares the experimental uptake with simulated CO_2 uptake, X, using the Weibull model at different temperature in 20% CO_2. In Figure 9, similar to a Weibull CDF, the normalized uptake initially began with a short slow ramping period, and then curved increasingly upward producing a concave shape. After the inflection point, the curve monotonically increased to one. Sánchez et al.[37] analyze the fitting capability of twenty-five probability distribution functions for distillation data of petroleum fractions. They concluded that the Weibull distribution was one of the best distribution functions for fitting sigmoidal or S-shape curve data, considering their ranking and the required central processing unit time.

Experimental values of a and b were obtained by curve fitting the uptake data presented in Figure 10 with the

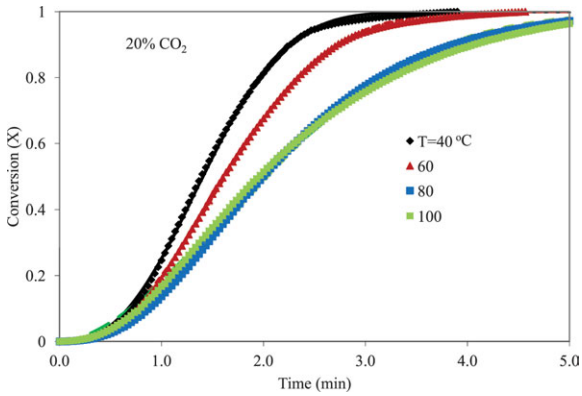

Figure 10. Comparison of experimental fractional uptake (marker) to Weibull reaction model (lines) at different temperature for 20% CO_2 concentration.

[Color figure can be viewed in the online issue, which is available at wileyonlinelibrary.com.]

expression in Eq. 8 using TABLECURVE available from SPSS. The typical fit of Eq. 8 to the CO_2 uptake, X, measurement is also illustrated in Figure 10. Agreement is very good over the entire experiment duration with overall variance explained (R^2) greater than 99%. The values determined for the shape parameter, b, range from 1.2 to 2.5 for all the temperature and CO_2 concentration measured; the average was $b = 1.97 \pm 0.18$ (95% CL). Figure 11 shows the shape parameter, b, for all the CO_2 concentrations as a function of reaction temperatures. The observed value of $b = 1.97$ was very close to the value of $b = 2$ that defines the Rayleigh distribution. The Rayleigh distribution is a special case of the Weibull function for modeling the lifetime of a device that has a linearly increasing instantaneous failure rate. To take advantage of the simplifications in the Rayleigh case, a value of $b = 2$ was used in this analysis. In the other extreme, when $b = 1$, Eq. 8 reduces to pseudo-first-order kinetics models. At high–temperatures, the b values approached unity and the kinetics simplify to a pseudo-first-order rate expression. This was consistent with the adsorption isotherms indicating a more homogeneous surface at higher-temperature. At lower-temperature, the b value approached 2.5, which reflects growth of nuclei with a constant nucleation rate. The values of the Weibull scale parameter, a, were recalculated based on the approximation of $b = 2$ for every set of uptake data taken at different temperatures and CO_2 concentration. Figure 12 compares the experimental fraction uptake with simulated fraction of CO_2 uptake, X, using $b = 2$ for the Rayleigh distribution for different concentrations at $T = 40$°C. Again, agreement is very good over the entire experiment duration with overall variance explained greater than 99.9%.

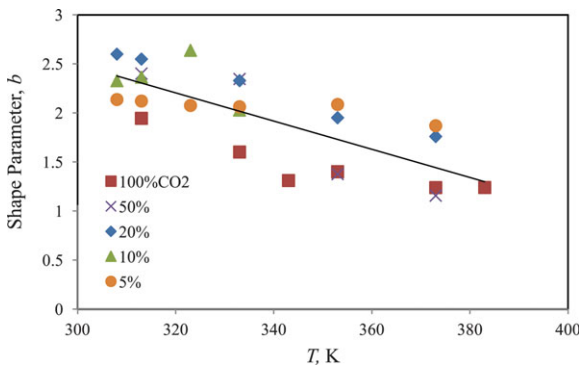

Figure 11. Variations of shape parameter of Weibull reaction model with reaction temperature and CO_2 concentration.

[Color figure can be viewed in the online issue, which is available at wileyonlinelibrary.com.]

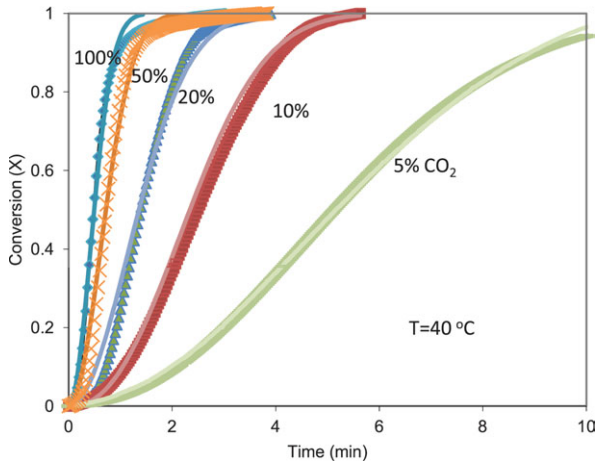

Figure 12. Comparison of fractional uptake to Weibull reaction model at different CO_2 concentration for $T = 40$°C.

[Color figure can be viewed in the online issue, which is available at wileyonlinelibrary.com.]

Since the time dependence of the extent of CO_2 uptake is well described by Eq. 8 and using $b = 2$, the corresponding rate can be given by first derivative of this function with respect to time as

$$\frac{dX}{dt} = 2ate^{-at^2} \tag{9}$$

Using Eq. 8, t can be obtained as

$$t = \sqrt{\frac{-\ln(1-X)}{a}} \tag{10}$$

By replacing t in Eq. 9, the rate can be solved independent of time as a function of temperature and uptake where a is a function of concentration and temperature.

$$\frac{dX}{dt} = 2a^{1/2}(1-X)\sqrt{-\ln(1-X)} \tag{11}$$

A differential equation can be derived in a form similar to Arrhenius form but using the modified Weibull CDF by substituting the temperature and concentration dependence of a into Eq. 11. To extract classical kinetic parameters, k was substituted into Eq. 11 using the definition:

$$k = 2a^{1/2} \tag{12}$$

and assuming an Arrhenius temperature dependence (Figure 13), $k = Ae^{(-E/RT)}$, where A is a pre-exponential factor, E is activation energy, R is a gas constant, and T is temperature in K. This analysis was consistent with the dimensional analysis

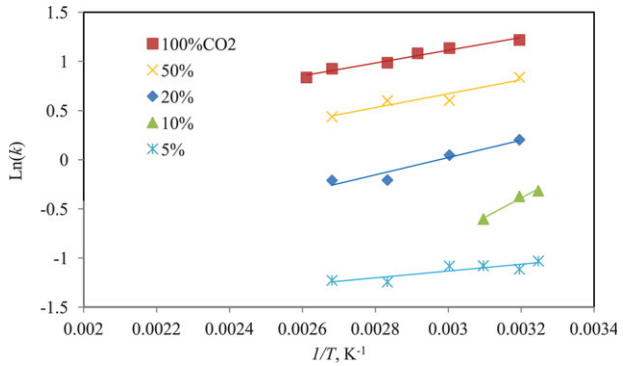

Figure 13. Temperature dependence of the Weibull reaction rate, *k* (1/min).

[Color figure can be viewed in the online issue, which is available at wileyonlinelibrary.com.]

(k is in min^{-1} while a is min^{-2}). The Arrhenius equation can be rewritten as

$$\ln k = \ln A - \frac{E}{RT} \tag{13}$$

From Eq. 13, it is apparent that the plot of $ln\ k$ vs. $1/T$ should result in a straight line with a slope of $-E/R$ and intercept of $ln\ A$. A plot of $ln(k)$ vs. $1/T$ for amine/silicate sorbent with particle size of 80 μm according to particle-CO_2 uptake is shown in Figure 13 for each reaction temperature and CO_2 concentrations between 5 and 100%. The values for pre-exponential factor, A, and activation energy, E, for the CO_2 removal were obtained from the intercept and slope of straight line in Figure 10. The values for A varied substantially as the CO_2 level changed, increasing with increasing CO_2. The temperature dependence for the activation energy, E, was fairly constant for different CO_2 levels as evidenced by the nearly parallel lines. Overall, for all of these CO_2 levels, the rate of reaction decreased as the temperature increased. This yielded the apparent negative activation energy. This finding was consistent with the negative temperature dependence observed by Ebner et al.[38] for similar sorbent.

Reactions with negative activation energies, though rare, have been noted with high frequency in some specific bimolecular reactions.[39–40] Reactions exhibiting negative activation energies are typically barrierless reactions, in which the reaction proceeding relies on the capture of the molecules in a potential well. Increasing the temperature leads to a reduced probability of the colliding molecules capturing one another (with more glancing collisions not leading to reaction as the higher momentum carries the colliding particles out of the potential well), expressed as a reaction cross-section that decreases with increasing temperature. Zellner and Lorenz[41] proposed an explanation in terms of collision theory if one assumes a cross-section, which increases rapidly at threshold energy, reaches a sharp maximum, and then decreases as energy is increased. Atkinson et al.[42] stated that it is possible that the activation energies are zero for the reaction of an OH radical with olefins and that the observed negative temperature dependences arise from a temperature dependence of the pre-exponential factor.

While the uptake of CO_2 is a low-energy process, it is not a barrierless process as described for free radical reactions. Thus, the rate controlling processes must be changing with temperature. This is often described as a change from kinetic to diffusion controlled process; thus, a Thiele modulus analysis was undertaken to evaluate the relative contributions of kinetic and diffusion processes on the overall rate. First, the kinetic rate constant, k, must be extracted from the temperature dependent data.

The order of the reaction was determined using non-linear regression of the rate data taken at different CO_2 concentrations (Figure 10). The PEI in the sorbent contains approximately 25% wt primary amine, 50% secondary, and 25% tertiary amine. The stoichiometry of CO_2 uptake reactions in Eq. 1 is 2:1 for primary and secondary amines. The stoichiometry is more complex with tertiary amines. A tertiary amine cannot react alone with carbon dioxide, but must react in concert with a hydrogen donor. In the presence of water, the tertiary amine reacts with CO_2 producing the tertiary ammonium bicarbonate, but in dry environment the PEI polymer reacts in concert with a primary or secondary amine. The CO_2:tertiary amine stoichiometry is 1:1. As a result, the theoretical reaction order for CO_2 can be calculated to be 0.625 for the PEI mixture. The reaction order of 0.693 ± 0.038 obtained from the analysis of the experimental data was consistent with that theoretical value.

Combining all the values of "k" and different CO_2 concentrations and placing them in Eq. 11, the following global rate equation was obtained

$$\frac{dX}{dt} = 0.42e^{\frac{662}{T}} y_{CO_2}^{0.693}(1-X)\sqrt{-\ln(1-X)} \tag{14}$$

The coefficients were taken as the average of the upper and lower limits for 95% confidence limits. The pre-exponential coefficient was $0.42 \pm 0.144\ min^{-1}$, and the temperature dependent coefficient was 662 ± 117 K. It is the square root term in Eq. 14 which leads to the sigmoidal response where the rate starts off slowly then increases to a peak as time progresses. It should be noted that the form of Eq. 14 is similar to JMA model that is used extensively in the field of nucleation and growth.[41] Thus, the two-step process of adsorbing CO_2 forming a zwitterion intermediate in this immobilized amine can be interpreted to proceed via a similar nucleation and growth process commonly found in polymerization processes.

The calculated rate–time (dX/dt vs. t) data obtained at different temperatures (Figure 14) show that the maximum rate of process obtained at $t > 0$. In Figure 14, the maximum rate decreased with the increasing temperature as observed in the experimental results (Figures 8 and 9); however, the changes in the induction period with temperature were more complex and could not be described as accurately. These variations in the induction period were not significant contribution to the overall rate. The calculated rate of reaction as a function of uptake is presented in Figure 15 for isothermal operating temperatures between 40 and 110°C. The rate increased with fractional uptake up to 40% uptake before dropping again as the active surface sites became depleted. This rate dropped systematically with temperature. Thus, the results from Figures 14 and 15 designated the sigmoid group of kinetic models (this group have $dX/dt_{,max}$ at $t > 0$, Case 2).

Theile Modulus Analysis. The sorption rate is not necessarily controlled by the rate of the kinetics reaction process

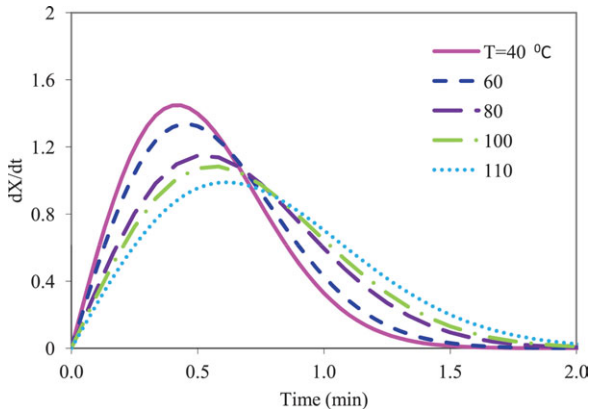

Figure 14. Effect of temperature on reaction rate using 100% CO_2.

[Color figure can be viewed in the online issue, which is available at wileyonlinelibrary.com.]

alone, but the rate in a porous media is a result of the (1) transport of reactants from the bulk fluid up to the adsorbent pellet, (2) transport of reactants from the external surface into the porous media (PEI), (3) adsorption, chemical reaction, and desorption of products at the sorbent sites, (4) transport of products from the sorbent interior to its external surface, and (5) transport of products into the bulk fluid. Usually one or at most two of the five steps are rate limiting and act to influence the overall rate of reaction in the pellet. The other steps are inherently faster than the slow step(s) and can accommodate any change in the rate of the slow step. The system is intra-particle transport controlled if step 2 is the slow process (sometimes referred to as diffusion limited). For kinetic or reaction control, step 3 is the slowest process. Finally, if step 1 is the slow process, the reaction is said to be externally transport controlled.

The effectiveness factor is widely used to account for the interaction between pore diffusion and reactions on pore walls in porous sorbent pellets and solid fuel particles. The effectiveness factor is a dimensionless sorption rate and is the ratio of the uptake rate actually observed to the uptake rate calculated if the surface sorbate concentration persisted throughout the interior of the particle. The uptake rate in a particle can, therefore, be conveniently expressed by its rate under surface conditions multiplied by the effectiveness factor. For a spherical particle, the effectiveness factor is generally defined as a function of the Thiele modulus ϕ[43]

$$\eta = \frac{1}{3\phi^2}\left(\frac{3\phi}{\tanh(3\phi)} - 1\right) \tag{15}$$

For a general nth-order reaction, the Thiele modulus is defined as[43]

$$\phi = \frac{d_p}{6}\left[\frac{(n+1)k^n RT}{2D_A^{\text{eff}}} P_{A,i}^{n-1}\right]^{1/2} \tag{16}$$

Note for small values of Thiele modulus, the reaction rate is small compared to the diffusion rate, and the sorbate concentration within the sorbent becomes nearly uniform. For large values of Thiele modulus, the reaction rate is large compared to the diffusion rate and the reactant is converted to product before it can penetrate very far into the pellet.

For the calculation of effective diffusivity, D_{eff}, two diffusion mechanisms must be taken into consideration inside the porous particles: bulk and Knudsen diffusion. D_{eff} can be computed using Bosanquet formula[44]

$$\frac{1}{D_{\text{eff}}} = \frac{1}{D_b} + \frac{1}{D_{\text{Kn}}} \tag{17}$$

where, D_{eff}, D_b, and D_{Kn} were calculated according to the following relation

$$D_b = \frac{\varepsilon D_m}{\tau} \tag{18}$$

$$D_m = 1.4 \times 10^{-5}\left(\frac{T}{273}\right)^{1.8} \tag{19}$$

$$D_{\text{Kn}} = 97 r_p \left(\frac{T}{\text{MW}}\right)^{1/2} \tag{20}$$

The tortuosity of the sorbent, τ, is unknown, but it appears that common values of tortuosity of microporous particles are of order of 2 and particle voidage were assumed to be a value of 0.25.

Using these estimates for diffusion rates of CO_2 into the sorbent and the reaction constant and order of reaction from Eq. 14, the Thiele modulus was calculated. The effectiveness factors were found to be 96–97% over the entire sorption-regeneration temperature range. Changing the assumed values for void fraction within the particle, τ, from 10 to 50% and tortuosity, τ, from 1 to 5 only changed the value of the estimated effectiveness factor by less than 10%. Thus, the Thiele modulus analysis confirmed that the process remained kinetically controlled over the entire temperature range under study. The lack of contribution from bulk and pore diffusion supports the conclusion that the active PEI was uniformly distributed on the substrate. Note that because the kinetic expression accounted for nucleation and growth mechanisms, these findings do not necessarily contradict the conclusion that adsorbate access was restricted to deeper layers of PEI at low-temperatures, nor do they exclude the possibility that

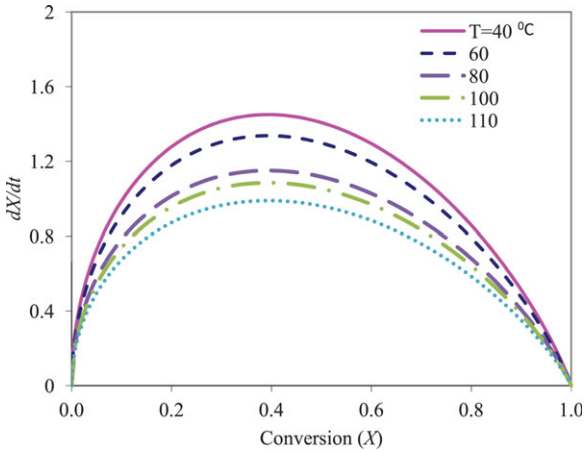

Figure 15. Effect of temperature on reaction rate as a function of fractional uptake using 100% CO_2.

[Color figure can be viewed in the online issue, which is available at wileyonlinelibrary.com.]

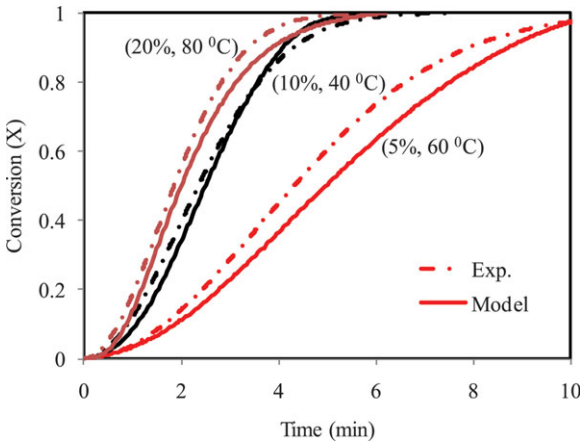

Figure 16. Comparison between kinetic model predictions and experimental data at several temperature and concentration in isothermal condition.

[Color figure can be viewed in the online issue, which is available at wileyonlinelibrary.com.]

mass transfer rates contribute to slowing the rate of nuclei growth during the later stages of the reaction.

The stoichiometry of a gas–solid reaction can be represented by

$$G_g + \alpha_s S_s \leftrightarrow \text{product} \tag{21}$$

where α_s is the stoichiometric coefficient associated with the solid reactant S. The rate of this reaction can be defined on the basis of gas or solid consumption, r_g and r_s, respectively. The rate expression on the basis of gas (CO_2) consumption

$$r_g = \frac{1}{m_0}\frac{dm_g}{dt} = \frac{dq}{dt} = q_e\frac{dX}{dt} \tag{22}$$

The following relation exists between r_s and r_g

$$r_s = (MW_s/MW_g)\alpha_s r_g \tag{23}$$

The kinetic and thermodynamic relationships were combined to demonstrate the ability to predict the overall response at different test conditions (Figure 16). The kinetic model was used to predict the fractional uptake for three test cases with combinations of different temperatures and CO_2 partial pressures. In general, there was good agreement between calculated and experimental results for all of these test cases. The expression developed here displayed the best agreement for higher CO_2 partial pressures because most of the experimental data was taken at those higher concentrations.

Summary

In this study, a rigorous approach has been taken to describe the kinetics, equilibrium, and thermodynamics of CO_2 uptake on immobilized PEI sorbent over the range of 303–383 K and five CO_2 concentrations: 5, 10, 20, 50, and 100%. The equilibrium data were analyzed using Langmuir, Temkin, Freundlich, and D–R isotherms. The characteristic parameters for each isotherm and related correlation coefficients were determined. The Temkin and Freundlich isotherm were demonstrated to provide the best correlation at lower-temperatures (40–60°C) and the Langmuir and D–R isotherms were the best fit at higher-temperatures (80–100°C). The temperature effect for the adsorption process and the thermodynamic parameters confirm the spontaneous character of the sorption reaction. The heat of adsorption from the Temkin and Freundlich isotherms indicates that the uptake process a mixture of ion exchange and physisorption.

The time-dependent uptake of CO_2 onto immobilized PEI sorbent was characterized to have peak rate at a time greater than zero, typical of Case 2 kinetics. The rate of CO_2 uptake under isothermal conditions decreased as temperature increased. This was interpreted to indicate that the rate controlling processes changed as the temperature changed. A phenomological kinetic model was developed to interpret this CO_2 uptake data taken in the TGA based on nucleation and growth mechanisms. This kinetic model was found to be quite successful. Because this model is used to describe nucleation and crystallization processes, it can be inferred that such processes control CO_2 uptake on this sorbent. Before nucleation, an induction period was observed, which generally decreased as the temperature increased. Using a Theile modulus analysis, it was found that CO_2 diffused rapidly through the macropores to interact with active surface sites. Nucleation can be thought to occur at the openings to the mesopores. This process was favored thermodynamically at lower-temperatures and decreased at higher-temperatures as reflected by the decrease in the shape factor b in the kinetic expression from 2.5 to 1.5 (Figure 11). In the later stages of the reaction growth of the product nuclei occurred by diffusion limited uptake of CO_2 with available active sites deeper in the mesopores. The rates of this process, though slower than the nucleation were observed to be faster at higher-temperature. However, the overall uptake was determined by the relatively fast rate of nucleation. The result was a negative temperature dependence such that the adsorption rate was faster at lower-temperature.

The kinetic model was used to predict the CO_2 uptake at different operating conditions and resulted in good agreement with experimental data. The results of present investigation show that immobilized PEI sorbent has considerable potential for the removal of CO_2 from flue gas over a wide range of concentration.

Acknowledgments

The authors acknowledge the Department of Energy for funding the research through the Fossil Energy's Carbon Sequestration/CO_2 Capture Research program.

Notation

a = Weibull scale parameter
b = Weibull shape parameter
B = heat of adsorption constant, $RT/-\Delta H_0$
CDF = cumulative distribution function
C_{CO2} = CO_2 concentration of gaseous product, mg/cm^3
D_b = bulk diffusivity, m^2/min
D_{eff} = effective diffusivity at bulk gas condition, m^2/min
D_{Kn} = Knudsen diffusivity, m^2/min
k = reaction rate constant, 1/min
K_F = Freundlich constant, mg/g
K_L = Langmuir adsorption constant, cm^3/mg
K_T = Temkin equilibrium binding constant, cm^3/mg
M_N = number average molecular weight, g/mole
MW = molecular weight, g/mol
PEI = polethylenimine
q = CO_2 uptake, mg-CO_2/g-sorbent
q_e = CO_2 uptake at pseudo-equilibrium, mg-CO_2/g-sorbent
q_m = maximum CO_2 uptake, mg-CO_2/g-sorbent

R = Universal gas constant, 1.985 cal/mol K
t = time of reaction, min
T = temperature, K
X = uptake
y_{CO_2} = CO_2 mole fraction

Greek letters

ε = particle voidage
η = effectiveness factor
φ = Thiele modulus at bulk gas condition
τ = tortuosity

Literature Cited

1. Song C. Global challenges and strategies for control, conversion and utilization of CO2 for sustainable development involving energy, catalysis, adsorption and chemical processing. *Catal Today*. 2006;115:2–32.
2. Adisorn A, Amornvadee V, Paitoon T. Behavior of the mass-transfer coefficient of structured packing in CO2 absorbers with chemical reactions. *Ind Eng Chem Res*. 1999;38:2044–2050.
3. Khatri RA, Chuang SSC, Soong Y, Gray M. Carbon dioxide capture by diamine-grafted SBA-15: a combined Fourier transform infrared and mass spectrometry study. *Ind Eng Chem Res*. 2005;44:3702–3708.
4. Tsuda T, Fujiwara T, Takteani Y, Saeguas T. Amino silica gels acting as a carbon dioxide absorbent. *Chem Lett*. 1992;21:2161–2164.
5. Knowles GP, Graham JV, Delaney SW, Chaffee AL. Aminopropyl-functionalized mesoporous silicas as CO2 adsorbents. *Fuel Process Technol*. 2005:86:1435–1448.
6. Harlick PJE, Sayari A. Applications of pore-expanded mesoporous silica triamine grafted material with exceptional CO_2 dynamic and equilibrium adsorption performance. *Ind Eng Chem Res*. 2007;46:446–458.
7. Gray ML, Soong Y, Champagne KL, Baltrus JRW, Stevens J, Toochinda P, Vhuang SSC. Carbon dioxide capture by amine-enriched fly ash carbon sorbents. *Sep Purif Technol*. 2004;35:31–36.
8. Siriwardane RV, Shen MS, Fisher EP, Poston JA. Adsorption of CO_2 on molecular sieves and activated carbon. *Energy Fuels*. 2001;15:279–284.
9. Monazam ER, Shadle LJ, Siriwardane RV. Equilibrium and absorption kinetics of carbon dioxide by solid supported amine sorbent. *AIChE J*. 2011;57:3153–3159.
10. Serna-Guerrero R, Sayari A. Modeling adsorption of CO2 on amine-functionalized mesoporous silica. 2: Kinetics and breakthrough curves. Chem Eng J. 2010;161:182–190.
11. Birbara PJ, Filburn TP, Nalette TA. U.S. Patent 6,364,938, 2006.
12. Xu X, Song C, Andrésen JM, Miller BG, Scaroni AW. Preparation and characterization of novel CO2''molecular basket'' adsorbents based on polymer-modified mesoporous molecular sieve MCM-4. *Microporous Mesoporous Mater*. 2003;62:29–45.
13. Crini G, Peindy NH, Gimbert F, Robert C. Removal of C.I. basic green 4, (malachite green) from aqueous solutions by adsorption using cyclodextrin-based adsorbent: kinetic and equilibrium studies. *Sep Purif Technol*. 2007;53:97–110.
14. Özacar M, Şengil Aİ. Adsorption of metal complex dyes from aqueous solutions by pine sawdust. *Bioresour Technol*. 2005;96:791–795.
15. Özacar M, Şengil Aİ. Adsorption of reactive dyes on calcined alunite from aqueous solutions. *J Hazard Mater*. 2003;B98:211–224.
16. Itodo AU, Happiness UO, Obaroh IO, Usman AU, Audu SS. Temkin, R-D, Langmuir and Freundlich adsorption isotherms of industrial dye uptake unto H3PO4 catalyzed poultry waste bioadsorbent. *J Sci Technol Res*. 2009b;8:52–56.
17. Temkin MJ, Pyzhev V. Recent modifications to Langmuir isotherms. *Acta Physiochim URSS*. 1940;12:217–222.
18. Gimbert F, Morin-Crini N, Renault F, Badot P, Crini G. Adsorption isotherm models for dye removal by cationized starch-based material in a single component system: error analysis. *J Hazard Mater*. 2008;157:34–46.
19. Munir K, Yusuf M, Noreen Z, Hameed A, Yusuf Hafeez F, Faryal R. Isothermal studies for determination of removal of bi-metal (Ni and Cr) ions by *Aspergillus niger*. *Pak J Bot*. 2010;42:593–604.
20. Horsfall M, Spiff AI, Abia AA. Studies on the influence of mercaptoacetic acid (MAA) modification of cassava (manihot sculenta cranz) waste biomass on the adsorption of Cu2+ and Cd2+ from aqueous solution. *Korean Chem Soc*. 2004;25:969–976.
21. Özcan S, Erdem B, Özcan A. Adsorption of Acid Blue 193 from aqueous solutions onto BTMA-bentonite. *Colloids Surf A*. 2005;266:73–81.
22. Šesták J.*Thermophysical Properties of Solids, Their Measurements and Theoretical Analysis*.Elsevier:Amsterdam, 1984.
23. Janković B. Isothermal reduction kinetics of nickel oxide using hydrogen: conventional and Weibull kinetics analysis. *J Phys Chem Solids*. 2007;68:2233–2246.
24. Burnham AK, Braun RL. Global kinetic analysis of complex material. *Energy Fuels*. 1999;13:1–22.
25. Šesták J, Berggren G. Study of the kinetics of the mechanism of solid-state reactions at increasing temperatures. *Thermochim Acta*. 1971;3:1–12.
26. Lo K-C, Wu K-T, Chyang C-S, Ting W-T. A new study on combustion behavior of pine sawdust characterized by the Weibull distribution. *Chin J Chem Eng*. 2009;17:860–868.
27. Málek J. The kinetic analysis of non-isothermal data. *Thermochim Acta*. 1992;200:257–269.
28. Ma X, Wang X, Song C. "Molecular basket" sorbents for separation of CO2 and H2S from various gas streams. *J Am Chem Soc*. 2009;131:5777–5783.
29. Gutowski K, Maginn EJ. Amine-functionalized task-specific ionic liquids: a mechanistic explanation for the dramatic increase in viscosity upon complexation with CO_2 from molecular simulation. *J Am Chem Soc*. 2008;130:14690–14704.
30. Kiran B, Kaushik A. Cyanobacterial biosorption of Cr (VI): application of two parameter and Bohart Adams models for batch and column studies. *Chem Eng J*. 2008;144:391–399.
31. Helfferich F. Kinetics. In: Helfferich, Friedrich G., *Ion-exchange*. New York: McGraw-Hill, 1962;250–319.
32. Zafar MN, Nadeem R, Hanif MA. Biosorption of nickel from protonated rice bran. *J Hazardous Mater*. 2007;143:478–485.
33. Wang X, Schwartz V, Clark JC, Ma X, Overbury SH, Xu X, Song C. Infrared study of CO2 sorption over "molecular basket" sorbent consisting of polyethylenimine-modified mesoporous molecular sieve. *J Phys Chem C*. 2009;113:7260–7268.
34. Málek J. The applicability of Johnson-Mehl-Avrami model in the thermal analysis of the crystallization kinetics of glasses. *Thermochim Acta*. 1995;267:61–73.
35. Weibull W. A statistical distribution functions of wide applicability. *J Appl Mech*. 1951;18:293–297.
36. Zhang H, Mitchell BS. A method for determining crystallization kinetic parameters from one nonisothermal calorimetric experiment. *J Mater Res*. 2000;15:1000–1007.
37. Sánchez S, Ancheyta J, McCaffrey J. Comparison of probability distribution functions for fitting distillation curves of petroleum. *Energy Fuels*. 2007;21:2955–2963.
38. Ebner AD, Gray ML, Chisholm NG, Black QT, Mumford DD, Nicholson MA, Ritter JA. Suitability of a solid amine sorbent for CO2 capture by pressure swing adsorption. *Ind Eng Chem Res*. 2011;50:5634–5641.
39. Mozurkewich M, Benson SW. Negative activation-energies and curved Arrhenius plots. 1. Theory of reactions over potential wells. *J Phys Chem*. 1984;88:6429–6435.
40. Mozurkewich M, Lamb JJ, Benson SW. Negative activation-energies and curved Arrhenius plots. 2. OH + CO. *J Phys Chem*. 1984;88:6435–6441.
41. Zellner R, Lorenz KJ. Laser photolysis resonance fluorescence study of the rate constants for the reaction of OH radicals with C2H4 and C3H6. *J Phys Chem*. 1984;88:984–989.
42. Atkinson R, Perry RA, Pitts JN. Rate constants for reaction of OH radicals with ethylene over temperature-range 299–425°K. *J Phys Chem*. 1977;66:1197–1201.
43. Veldsink JW, Versteeg GF, van Swaaij WPM. Intrinsic kinetics of the oxidation of methane over an industrial copper(I1) oxide catalyst on a γ-alumina support. *Chem Eng J*. 199;57:273–283.
44. Mani T, Mahinpey N, Murugan P. Reaction kinetics and mass transfer studies of biomass char gasification with CO2. *Chem Eng Sci*. 2011;66:36–41.

Manuscript received Dec. 21, 2011, and revision received May 18, 2012.